Polymers **2015**, *7*, 1221-1231; doi:10.3390/polym7071221

OPEN ACCESS

polymers

ISSN 2073-4360

www.mdpi.com/journal/polymers

Article

Thermal Conductivity and Specific Heat Capacity of Dodecylbenzenesulfonic Acid-Doped Polyaniline Particles—Water Based Nanofluid

Tze Siong Chew [1], Rusli Daik [1,*] and Muhammad Azmi Abdul Hamid [2]

[1] School of Chemical Sciences and Food Technology, Faculty of Science and Technology, Universiti Kebangsaan Malaysia, UKM Bangi Selangor 43600, Malaysia; E-Mail: chewtzesiong0203@gmail.com

[2] School of Applied Physics, Faculty of Science and Technology, Universiti Kebangsaan Malaysia, Bangi Selangor 43600, Malaysia; E-Mail: azmi@ukm.edu.my

* Author to whom correspondence should be addressed; E-Mail: rusli.daik@ukm.edu.my; Tel.: +603-8921-5412; Fax: +603-8921-5410.

Academic Editor: Patrick Ilg

Received: 28 April 2015 / Accepted: 25 June 2015 / Published: 7 July 2015

Abstract: Nanofluid has attracted great attention due to its superior thermal properties. In this study, chemical oxidative polymerization of aniline was carried out in the presence of dodecylbenzenesulfonic acid (DBSA) as a dopant. Particles of DBSA-doped polyaniline (DBSA-doped PANI) with the size range of 15 to 50 nm were obtained, as indicated by transmission electron microscope (TEM). Results of ultra violet-visible (UV-Vis) absorption and Fourier transform infrared (FTIR) spectroscopies as well as thermogravimetric analysis showed that PANI nanoparticles were doped with DBSA molecules. The doping level found was 36.8%, as calculated from elemental analysis data. Thermal conductivity of water was enhanced by 5.4% when dispersed with 1.0 wt% of DBSA-PANI nanoparticles. Specific heat capacity of water-based nanofluids decreased with increasing amount of DBSA-PANI nanoparticles.

Keywords: conjugated polymer; nanomaterials; polymer colloid; doping; surfactant

1. Introduction

Nanotechnology and nanomaterials offer vast potential in various applications, such as transportation, micromechanics and instrumentation, heating, ventilating and air conditioning (HVAC), medical, and solar energy [1–3]. A nanofluid is a kind of colloidal dispersion achieved by dispersing nanoparticles in a base fluid [4]. They have excellent thermosphysical properties, such as thermal conductivity, specific heat capacity, thermal diffusivity, viscosity, and convective heat transfer coefficients [5].

Fluids containing particles with diameter range of micrometer or millimeter usually have problems in terms of particle sedimentation, clogging of flow channels, erosion of pipelines and pressure drop. Whereas, nanofluids have better stability, higher thermal conductivity, less clogging problem and less pressure drop. The size of heat transfer system can also be reduced with better heat transfer characteristics [6,7].

Preparation method of nanofluids is crucial in order to ensure a good dispersion of nanoparticles in base fluids so that the thermophysical properties may be improved. Generally, there are two methods of preparation, namely single-step method and two-step method. The single-step method is a process that combines synthesis of nanoparticles and preparation of nanofluids [8]. The agglomeration of nanoparticles can be reduced since drying, storage, transportation and dispersion of nanoparticles are avoided [9]. However, it is highly impractical to be applied at industrial scale [6]. Two-step method involves the synthesis of nanoparticles and preparation of nanofluids separately. It can be scaled up for industrial purposes; however, agglomeration and clustering of nanoparticles are inevitable and affect the stability of nanofluids [10,11]. Hence, preparation of stable nanofluids using two-step method becomes a major challenge.

In nanofluids, agglomeration of nanoparticles is usually ascribed to van der Waals interaction between particles. This can be overcome by subjecting them to ultra-sonification [12,13]. Besides, adding surfactant or activator to modify the hydrophobic surfaces of nanoparticles to become hydrophilic for aqueous and vice versa can also be used for non-aqueous [14,15]. In addition, pH control can create a strong repulsive force that can stabilize a well-dispersed suspension [16,17].

Recently, development of water-based nanofluids has been highlighted. The enhancement in thermal conductivity of water was achieved when the amount of dispersed carbon nanotubes was increased [18,19]. It was also reported that 5% volume fraction of TiO_2 nanoparticles and 7.5% of volume fraction of CuO enhanced thermal conductivity of water by 33% and 32%, respectively [20,21], whereas 5% volume of ZnO enhanced thermal conductivity of water by 12% [22]. So far, several mechanisms of thermal conductivity enhancement of nanofluids has been proposed, such as the Brownian motion of nanoparticles [23], molecular-level layering of the liquid at the liquid particle interface [24], the nature of heat transport in the nanoparticles, and the effect of nanoparticle clustering [25].

Among the various types of polymer, polyaniline (PANI) is a popular conductive polymer due to its environmental stability, lower cost and easy production. PANI becomes conductive through doping. Han *et al.*, [26] successfully synthesized dodecylbenzenesulfonic acid (DBSA)-doped PANI nanoparticles with an average size of 20–30 nm using direct micelle polymerization. Han *et al.*, [27] synthesized uniform needle shape of DBSA-doped PANI nanoparticles using isooctane as continuous phase. The synthesis of DBSA-doped PANI nanoparticles in hexane has also been reported using one-step reverse micelle polymerization [28].

So far, inorganic and oxide nanoparticles are commonly used in the preparation of nanofluids. To the best of our knowledge, water based nanofluid containing DBSA-doped PANI nanoparticles has not yet been explored. In this study, we aimed at producing water-based nanofluid with DBSA-doped PANI nanoparticles as the dispersed phase. Thermal conductivity and specific heat capacity of DBSA-doped PANI nanoparticles water-based nanofluids were studied.

2. Experimental Section

2.1. Materials

Aniline (Ani) was purified by passing through an alumina column to remove moisture and inhibitor. The purified Ani was stored in a refrigerator prior to use. Dodecylbenzenesulfonic acid (DBSA), ammonium peroxylsulfate (APS) and isooctane were used without further purification. All chemicals were purchased from Acros Organic (Themo Fisher Scientific: Fair Lawn, NJ, USA). Deionized water was used throughout the experiment.

2.2. Synthesis of DBSA-Doped PANI Nanoparticles

In a typical synthesis of DBSA-doped PANI, 2.28 g of APS was dissolved in 5.0 mL of deionized water, while 13.05 g of DBSA was dissolved in 50 mL of isooctane. Solutions of APS and DBSA were mixed to form (A) solution. The solution A was stirred for 30 min at room temperature. Aniline (1.86 g) was added into 10 mL of isooctane and 1.0 mL of ethanol to produce another homogenous solution (B). The solution B was added into the solution A and the mixture was stirred for 24 h at room temperature. The dark green precipitate was washed with deionized water and methanol, filtered and dried in a vacuum oven for 24 h. Then, 2.5 g DBSA-doped PANI was dedoped in 500 mL of ammonia solution for 24 h at room temperature to yield emeraldine base polyaniline (EB-PANI).

2.3. Preparation of Nanofluid of DBSA-Doped PANI Nanoparticles and Water

Polymer nanofluids were physically prepared by dispersing DBSA-doped PANI nanoparticles in deionized water using micro mass balance (model Sartorius TE2145, Sartorius AG: Göttingen, Germany) with S.D. = 0.1 mg. The weight percentage of DBSA-doped PANI nanoparticles was fixed in range of 0.2% to 1.0%. Polymer nanofluid (0.2 wt%): 0.02 g of DBSA-doped PANI nanoparticles was dispersed in 9.98 g of deionized water using a 24 kHz ultrasonic bath (Elmasonic P: Singen, Germany) of 80 W for 8 h. The pH of water was adjusted to pH 8 by 0.1 M NaOH.

2.4. Characterization of DBSA-Doped PANI Nanoparticles

The morphology and size of DBSA-doped PANI nanoparticles were investigated by FESEM SUPRA 55VP (Carl Zeiss Microscopy GmbH: Zeiss, Germany). The size of DBSA-doped PANI nanoparticles was also studied using TEM (FEI company: Hillsboro, OR, USA). The sample was dispersed in methanol and sonicated for 10 min. The FTIR spectra of samples was investigated on a Perkin Elmer Spectrum (Perkin Elmer GX: Waltham, MA, USA), over a frequency range of 400–4000 cm^{-1} at a scanning resolution of 4 cm^{-1}. Samples were pelletized using KBr. The UV-Vis absorption spectra of

samples were recorded using UV-Vis spectroscopy 1650PC, (Shimadzu Europa GmbH: Duisburg, Germany) over a wavelength range of 200 to 800 nm. The samples were dissolved in DMSO (dimethyl sulfoxide). The elemental compositions of C, H, N and S were identified by elemental analyzer LECO CHNS-932 model (LECO Corporation: St. Joseph, MI, USA) and FISION EA 1108 model (Fisons Plc.: Ipswich, UK). Based on the obtained composition of elements, doping level of DBSA-doped PANI could be determined. TGA analysis was carried out using TGA/SDTA 851 model (Mettler-Toledo: Schwerzenbach, Switzerland) to determine the thermal stability of the synthesized polymers. The sample was heated from room temperature to 800 °C with nitrogen flow and heating rate of 10 °C/min.

2.5. Stability of Nanofluids

The hydrodynamic size distribution of nanofluids was measured by Zeta Sizer (Nano-ZS, Malvern Instruments: Malvern, UK), which works on the principle of dynamic light scattering. Deionized water containing 0.1% of DBSA-doped PANI nanoparticles was measured. The hydrodynamic size distribution reflected stability of suspension.

2.6. Thermal Conductivity Measurement of Nanofluid

Thermal conductivity of the nanofluid was measured using Thermal Properties Analyzer KD2 Pro. (Decagon Devices Incorporation: Pullman, WA, USA). The KD2 is based on transient hot wire method having a single probe of length 6 cm and diameter 1.3 cm. The KD2 analyzer was calibrated by using deionized water and glycerin prior to use. Thermal conductivity was obtained directly from the digital readout after it was operating based on the line heat source method. The measurements were taken over the weight percentage of filler of 0.2%, 0.4%, 0.6%, 0.8% and 1.0% at room temperature. Ten measurements were taken for each sample.

2.7. Specific Heat Capacity Measurement of Nanofluid

The specific heat capacity of PANI nanoparticles/water nanofluids was determined by using differential scanning calorimetry, (DSC) 823 model (Mettler Toledo: Schwerzenbach, Switzerland). Firstly, the measurement was taken with two empty samples to obtain a baseline. After the reference curve was obtained by using a pan containing sapphire standard disc and an empty pan, the measurement on a pan containing sample and an empty pan was carried out. The heating was performed at temperature of 25 to 80 °C with 20 °C/min heating rate. The heating procedure consisted of three steps: (1) Equilibrate and remain isothermal at 25 °C for 4 min; (2) Ramp to 80 °C at 20 °C/min; and (3) Remain isothermal at 80 °C for 4 min.

3. Results and Discussion

3.1. FTIR Characterizations of DBSA-PANI Nanoparticles

The mass recovery of the dark greenish DBSA-doped PANI is 93.2%. As shown in Figure 1a,b, uniform spherical DBSA-doped PANI nanoparticles were successfully synthesized via reverse micellar

polymerization. The size range of nanoparticles was 15 to 50 nm. At the same time, agglomeration of some DBSA-doped PANI nanoparticles was observed.

The peaks at 3393, 2916, 1031, and 1006 cm^{-1} could be assigned to O–H stretching, C–H stretching of $–CH_2$, S=O stretching and >CH stretching of benzenoid rings in DBSA molecule, respectively. These peaks were also observed in DBSA-doped PANI but were not present in EB-PANI. This indicated that PANI was successfully doped with DBSA molecules.

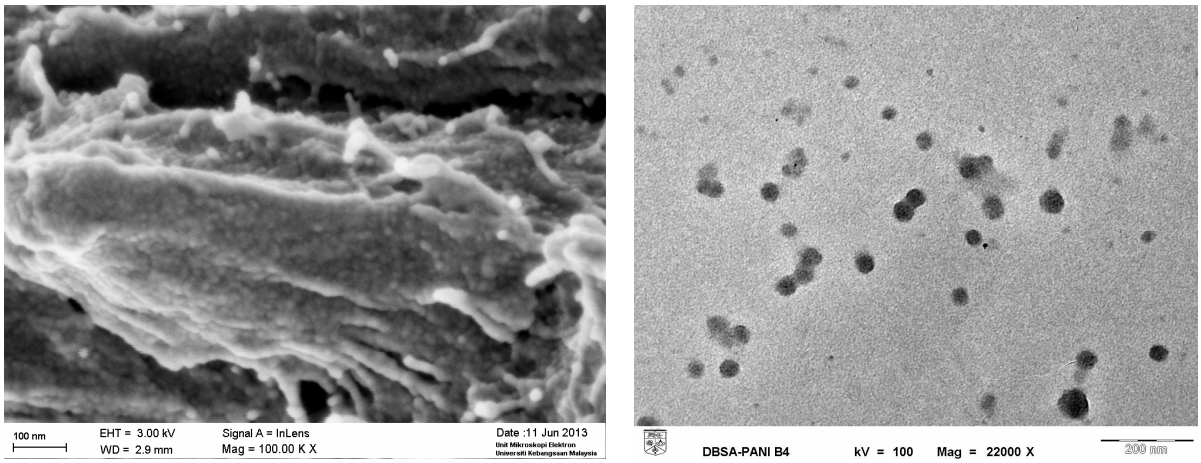

Figure 1. (**a**) FESEM micrograph of DBSA-doped PANI (dodecylbenzenesulfonic acid-doped polyaniline); and (**b**) TEM micrograph of DBSA-doped PANI.

FTIR spectra of DBSA, EB-PANI and DBSA-doped PANI are shown in Figure 2. The bands near 1567 cm^{-1} and 1460 cm^{-1} were assigned to C=C in benzenoid rings and in quinoid rings of DBSA-doped PANI and EB-PANI. The C–N stretching of secondary amine of PANI backbone was observed at 1293 cm^{-1}. Mode of N=Q=N was indicated by the peak of 1116 cm^{-1}. It was formed during protonation.

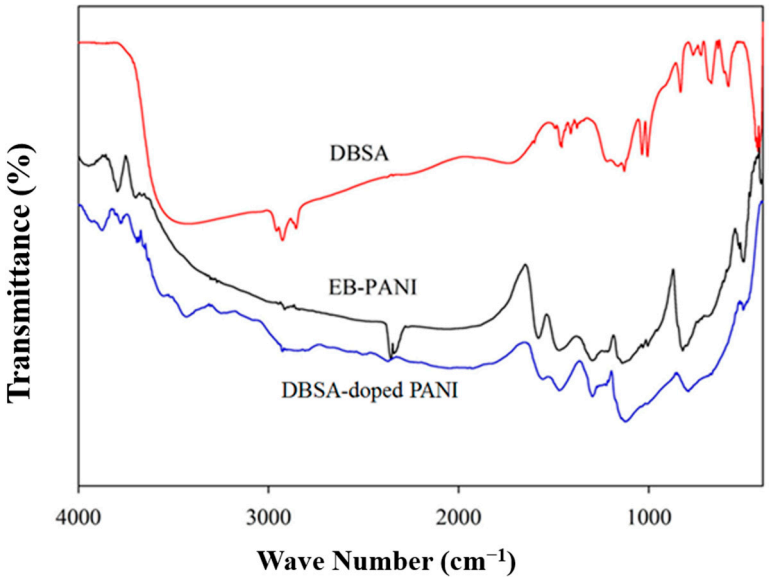

Figure 2. FTIR spectra of DBSA (dodecylbenzenesulfonic acid), EB-PANI (emeraldine base polyaniline) and DBSA-doped PANI (dodecylbenzenesulfonic acid-doped polyaniline).

The UV-Visible absorption spectra of EB-PANI, DBSA-doped PANI and DBSA in DMSO were shown in Figure 3. The excitation of benzenoid rings of polymer backbone was at 326 nm for EB-PANI and DBSA-doped PANI. However, the peak of quinoid rings of EB-PANI was observed at 628 nm. This peak was absent in the spectrum of DBSA-doped PANI because the quinoid rings were affected by the presence of DBSA molecules. The peak observed at 257 nm was assigned to π→π* transition in the benzenoid rings of DBSA. This peak was also present in DBSA-doped PANI, thus implying that DBSA was successfully doped into PANI.

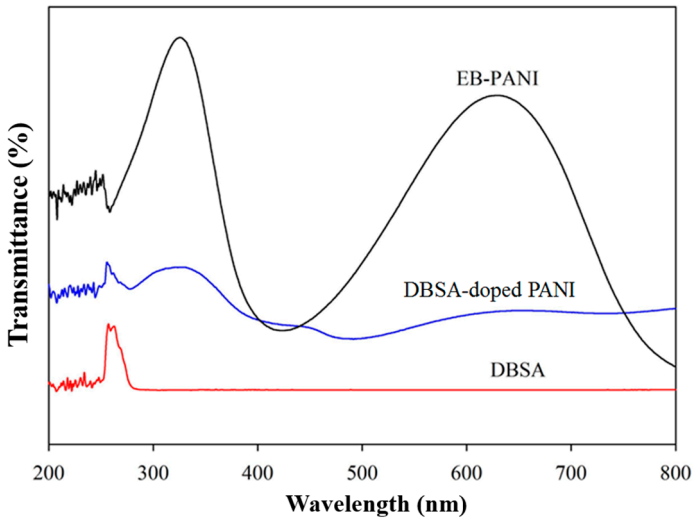

Figure 3. UV-Visible absorption spectra of EB-PANI, DBSA-doped PANI and DBSA.

As seen in Table 1, EB-PANI was free of sulfur, as expected. This showed that EB-PANI was successfully dedoped using 5% of ammonia solution. The doping level was determined according to Equation (1). Each repeat unit contains one nitrogen atom while each DBSA molecule contains one sulfur atom. Thus, ratio of S/N was used to calculate the level of DBSA doping into PANI chains. The doping level found was 36.8%.

$$\text{Doping level (\%)} = \frac{S}{N} \times \frac{1}{2.286} \times 100 \quad (1)$$

where *S* is the elemental composition of sulfur in sample and *N* is the elemental composition of nitrogen in sample.

Table 1. Elemental composition of EB-PANI and DBSA-doped PANI.

Composition	EB-PANI (%)	DBSA-Doped PANI (%)
Carbon	71.3	65.5
Hydrogen	8.6	8.7
Nitrogen	16.2	6.4
Sulfur	–	5.4
Oxygen	3.9	14.0

Notes: EB-PANI, emeraldine base polyaniline; DBSA-doped PANI, dodecylbenzenesulfonic acid-doped polyaniline.

TGA thermograms of EB-PANI and DBSA-doped PANI (Figure 4) showed that the first stage of weight loss occurred below 100 °C, and this could be related to evaporation of water molecules from

EB-PANI and DBSA-doped PANI. The second weight loss, which was only observed for DBSA-doped PANI, occurred at higher temperature, from 210 to 295 °C. It was assigned to loss of DBSA dopants from DBSA-doped PANI. The third weight loss was due to the decomposition of PANI chains itself. It started at 310 °C and ended at 680 °C. TGA results were in good agreement with those of FTIR and UV-Vis absorption spectroscopies as well as elemental analysis. It could therefore be concluded that the synthesis of DBSA-doped PANI nanoparticles was successful and the doping was proven to take place only in emeraldine state.

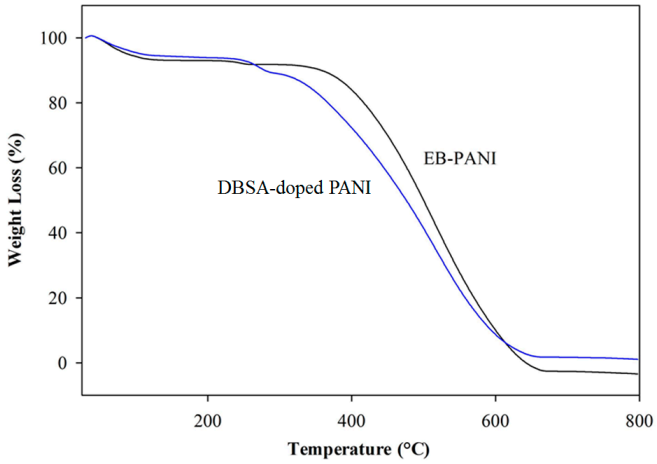

Figure 4. TGA thermograms of EB-PANI and DBSA-doped PANI.

3.2. Stability of Nanofluids

Figure 5 showed the size distribution of 0.1 wt% of DBSA-doped PANI nanoparticles dispersed in water. The size range of DBSA-doped PANI nanoparticles was from 120 to 400 nm with a mean value of 230 nm. The size of DBSA-doped PANI nanoparticles became larger when it was dispersed in water. DBSA-doped PANI nanoparticles tend to agglomerate and settle down in water after 2 h due to hydrodynamic effect and strong force of attraction between the solid nanoparticles due to their high surface area. In addition, long hydrocarbon segments, $CH_3(CH_2)_{11}(C_6H_4)$, of DBSA would interact poorly with water [29]. The agglomeration of nanoparticles would ultimately lead to destabilization of nanofluid.

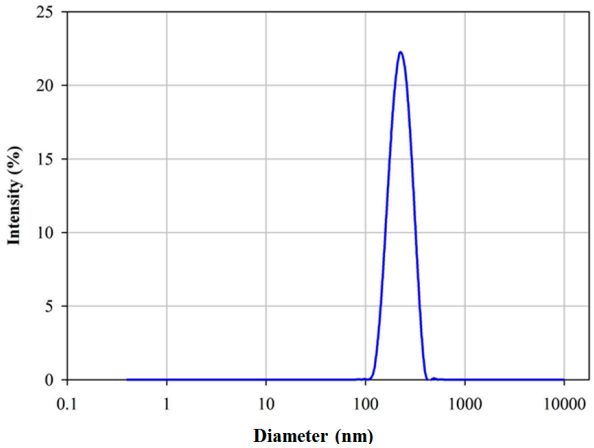

Figure 5. Size distribution of 0.1 wt% of DBSA-doped PANI nanoparticles dispersed in water.

3.3. Thermal Conductivity of Nanofluids

Table 2 shows the thermal conductivity of nanofluids with various mass fractions of DBSA-doped PANI nanoparticles. It could be observed that when mass fraction of DBSA-doped PANI nanoparticles was increased, the thermal conductivity of nanofluids increased. The increase was possibly related to the Brownian motion of nanoparticle [23,30]. It was reported that the Brownian motion effect of nanoparticles on thermal conductivity was more pronounced at low mass fraction of nanoparticles [31]. However, in this case, the increase in thermal conductivity was rather small compared to the one containing inorganic or oxide nanoparticles [21,32,33]. It is anticipated that polyaniline as well as DBSA molecules (doped DBSA) could interact with water molecules to form hydrogen bonding [34]. Interaction between doped DBSA and water may have resulted in a redistribution of charge on the backbone in the direction of the equilibrium distribution of bare radical cation [35]. Doped DBSA with long hydrocarbon tails could lessen the polar character of polymer chains [36]. It was believed that interaction between dopants and base liquid was a significant factor affecting the thermal conductivity of nanofluid in this study.

Table 2. Thermal conductivity and enhancement in thermal conductivity for water based nanofluids at different mass fraction of DBSA-PANI nanoparticles.

Mass Fraction of DBSA-PANI Nanoparticles (%)	Thermal Conductivity (W/m·K)	Enhancement in Thermal Conductivity (%)
0	0.596 ± 0.018	–
0.2	0.602 ± 0.018	1.0
0.4	0.604 ± 0.024	1.4
0.6	0.607 ± 0.004	1.9
0.8	0.616 ± 0.019	3.4
1.0	0.628 ± 0.012	5.4

3.4. Specific Heat Capacity of Nanofluids

Plots of specific heat capacity of nanofluids with various mass fractions of DBSA-doped PANI nanoparticles are shown in Figure 6. Specific heat capacity of nanofluid decreased when the mass fraction of DBSA-doped PANI nanoparticles increased. However, specific heat capacity nanofluids increased with increasing temperature. Decrease of specific heat capacity was reported for various water-based metallic and inorganic nanofluid systems [37–40]. Solid–liquid interface interaction was crucial for energy storage and will change the phonon vibration mode between solid and fluid [40]. In this study, solid–liquid interface was formed between DBSA-doped PANI nanoparticles and water molecules. This type of interaction could change the specific heat capacity of water. Hydrogen bonding established between doped DBSA and water contributed further to the heat transfer. Hence, less thermal energy was stored when more DBSA-doped PANI nanoparticles dispersed in water.

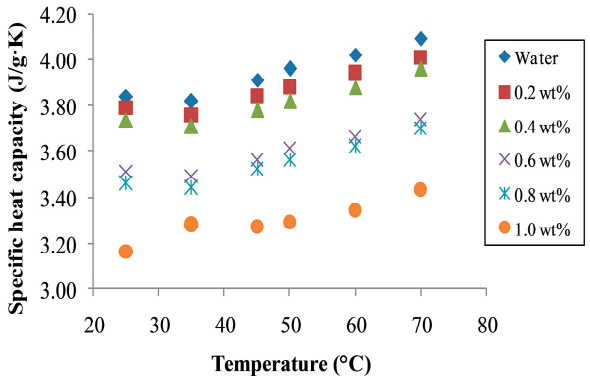

Figure 6. Specific heat capacity of nanofluids with various mass fractions of DBSA-doped PANI nanoparticles.

4. Conclusions

DBSA-doped PANI nanoparticles were successfully synthesized via reverse micellar polymerization. Increase in thermal conductivity and decrease in specific heat capacity of nanofluids were dependent on mass fraction of DBSA-doped PANI nanoparticles. An increase of 5.4% in thermal conductivity of water was obtained when dispersed with 1.0 wt% DBSA-doped PANI nanoparticles. DBSA as a dopant was shown to have a significant effect on thermal conductivity as well as specific heat capacity of nanofluids.

Acknowledgments

Authors gratefully acknowledge financial support from Malaysia Ministry of Education (ERGS/1/2013/STG01/UKM/02/5).

Author Contributions

Tze Siong Chew carried out the experimental work and analysis under the supervision of Rusli Daik and Muhammad Azmi Abdul Hamid.

Conflicts of Interest

The authors declare no conflict of interest.

References

1. Murshed, S.M.S.; Leong, K.C.; Yang, C. Thermophysical and electrokinetic properties of nanofluids—A critical review. *Appl. Therm. Eng.* **2008**, *28*, 2109–2125.
2. Saidur, R.; Leong, K.Y.; Mohammad, H.A. A review on applications and challenges of nanofluids. *Renew. Sustain. Energy Rev.* **2011**, *15*, 1646–1668.
3. Mahian, O.; Kianifar, A.; Kalogirou, S.A.; Pop, I.; Wongwises, S. A review of the applications of nanofluids in solar energy. *Int. J. Heat Mass Transf.* **2013**, *57*, 582–594.
4. Choi, S.U.S.; Eastman, J.A. Enhancing thermal conductivity of fluids with nanoparticles. In Proceedings of the ASME International Mechanical Engineering Congress & Exposition, San Francisco, CA, USA, November 1995; pp. 99–105.

5. Xu, W.; Xie, H. A review on nanofluids: Preparation, stability mechanisms, and applications. *J. Nanomater.* **2011**, *2012*, doi:10.1155/2012/435873
6. Li, Y.; Zhou, J.; Tung, S.; Schneider, E.; Xi, S. A review on development of nanofluid preparation and characterization. *Powder Technol.* **2009**, *196*, 89–101.
7. Ghadimi, A.; Saidur, R.; Metselaar, H.S.C. A review of nanofluid stability properties and characterization in stationary conditions. *Int. J. Heat Mass Transf.* **2011**, *54*, 4051–4068.
8. Liu, M.-S.; Lin, M.C.-C.; Tsai, C.Y.; Wang, C.-C. Enhancement of thermal conductivity with Cu for nanofluids using chemical reduction method. *Int. J. Heat Mass Transf.* **2006**, *49*, 3028–3033.
9. Zhu, H.-T.; Lin, Y.-S.; Yin, Y.-S. A novel one-step chemical method for preparation of copper nanofluids. *J. Colloid Interface Sci.* **2004**, *277*, 100–103.
10. Tantra, R.; Tompkins, J.; Quincey, P. Characterisation of the de-agglomeration effects of bovine serum albumin on nanoparticles in aqueous suspension. *Colloids Surfaces B* **2010**, *75*, 275–281.
11. Gu, B.; Hou, B.; Lu, Z.; Wang, Z.; Chen, S. Thermal conductivity of nanofluids containing high aspect ratio fillers. *Int. J. Heat Mass Transf.* **2013**, *64*, 108–114.
12. Chung, S.J.; Leonard, J.P.; Nettleship, I.; Lee, J.K.; Soong, Y.; Martello, D.V.; Chyu, M.K. Characterization of ZnO nanoparticle suspension in water: Effectiveness of ultrasonic dispersion. *Powder Technol.* **2009**, *194*, 75–80.
13. Tajik, B.; Abbassi, A.; Saffar-Avval, M.; Najafabadi, M.A. Ultrasonic properties of suspensions of TiO_2 and Al_2O_3 nanoparticles in water. *Powder Technol.* **2012**, *217*, 171–176.
14. Ghadimi, A.; Metselaar, I.H. The influence of surfactant and ultrasonic processing on improvement of stability, thermal conductivity and viscosity of titania nanofluid. *Exp. Therm. Fluid Sci.* **2013**, *51*, 1–9.
15. Meibodi, M.E.; Vafaie-Sefti, M.; Rashidi, A.M.; Amrollahi, A.; Tabasi, M.; Kalal, H.S. The role of different parameters on the stability and thermal conductivity of carbon nanotube/water nanofluids. *Int. Commun. Heat Mass Transf.* **2010**, *37*, 319–323.
16. Suganthi, K.S.; Rajan, K.S. Temperature induced changes in ZnO–water nanofluid: Zeta potential, size distribution and viscosity profiles. *Int. J. Heat Mass Transf.* **2012**, *55*, 7969–7980.
17. Iranidokht, V.; Hamian, S.; Mohammadi, N.; Shafii, M.B. Thermal conductivity of mixed nanofluids under controlled pH conditions. *Int. J. Therm. Sci.* **2013**, *74*, 63–71.
18. Halelfadl, S.; Maré, T.; Estellé, P. Efficiency of carbon nanotubes water based nanofluids as coolants. *Exp. Therm. Fluid Sci.* **2014**, *53*, 104–110.
19. Estellé, P.; Halelfadl, S.; Maré, T. Thermal conductivity of CNT water based nanofluids: Experimental trends and models overview. *J. Therm. Eng.* **2015**, *1*, 381–390.
20. Murshed, S.; Leong, K.; Yang, C. Enhanced thermal conductivity of TiO—Water based nanofluids. *Int. J. Therm. Sci.* **2005**, *44*, 367–373.
21. Khedkar, R.S.; Sonawane, S.S.; Wasewar, K.L. Influence of Cuo nanoparticles in enhancing the thermal conductivity of water and monoethylene glycol based nanofluids. *Int. Commun. Heat Mass Transf.* **2012**, *39*, 665–669.
22. Jeong, J.; Li, C.; Kwon, Y.; Lee, J.; Kim, S.H.; Yun, R. Particle shape effect on the viscosity and thermal conductivity of ZnO nanofluids. *Int. J. Refrig.* **2013**, *36*, 2233–2241.
23. Xiao, B.; Yang, Y.; Chen, L. Developing a novel form of thermal conductivity of nanofluids with brownian motion effect by means of fractal geometry. *Powder Technol.* **2013**, *239*, 409–414.

24. Xue, L.; Keblinski, P.; Phillpot, S.; Choi, S.-S.; Eastman, J. Effect of liquid layering at the liquid–solid interface on thermal transport. *Int. J. Mass Transf.* **2004**, *47*, 4277–4284.
25. Kole, M.; Dey, T. Role of interfacial layer and clustering on the effective thermal conductivity of CuO-Gear oil nanofluids. *Exp. Therm. Fluid Sci.* **2011**, *35*, 1490–1495.
26. Han, M.G.; Cho, S.K.; Oh, S.G.; Im, S.S. Preparation and characterization of polyaniline nanoparticles synthesized from DBSA micellar solution. *Synth. Metals* **2002**, *126*, 53–60.
27. Han, D.; Chu, Y.; Yang, L.; Liu, Y.; Lv, Z. Reversed micelle polymerization: A new route for the synthesis of DBSA–polyaniline nanoparticles. *Colloids Surfaces A* **2005**, *259*, 179–187.
28. Han, Y.-G.; Kusunose, T.; Sekino, T. One-step reverse micelle polymerization of organic dispersible polyaniline nanoparticles. *Synth. Metals* **2009**, *159*, 123–131.
29. MacDiarmid, A.; Epstein, A.J. The concept of secondary doping as applied to polyaniline. *Synth. Metals* **1994**, *65*, 103–116.
30. Wan, M.; Yadav, R.; Yadav, K.; Yadaw, S. Synthesis and experimental investigation on thermal conductivity of nanofluids containing functionalized polyaniline nanofibers. *Exp. Therm. Fluid Sci.* **2012**, *41*, 158–164.
31. Haddad, Z.; Abu-Nada, E.; Oztop, H.F.; Mataoui, A. Natural convection in nanofluids: Are the thermophoresis and Brownian motion effects significant in nanofluid heat transfer enhancement? *Int. J. Therm. Sci.* **2012**, *57*, 152–162.
32. Liu, M.; Lin, M.C.; Wang, C. Enhancements of thermal conductivities with Cu, CuO, and carbon nanotube nanofluids and application of MWNT/water nanofluid on a water chiller system. *Nanoscale Res. Lett.* **2011**, *6*, 1–13.
33. Karthik, V.; Sahoo, S.; Pabi, S.; Ghosh, S. On the phononic and electronic contribution to the enhanced thermal conductivity of water-based silver nanofluids. *Int. J. Therm. Sci.* **2013**, *64*, 53–61.
34. Łużny, W.; Piwowarczyk, K. Hydrogen bonds in camphorsulfonic acid doped polyaniline. *Polimery* **2011**, *56*, 652–656.
35. Shacklette, L. Dipole and hydrogen-bonding interactions in polyaniline: A mechanism for conductivity enhancement. *Synth. Metals* **1994**, *65*, 123–130.
36. Zhang, L.; Long, Y.; Chen, Z.; Wan, M. The effect of hydrogen bonding on self-assembled polyaniline nanostructures. *Adv. Funct. Mater.* **2004**, *14*, 693–698.
37. Jung, S.; Jo, B.; Shin, D.; Banerjee, D. Experimental validation of a simple analytical model for specific heat capacity of aqueous nanofluids. *Development* **2010**, *1*, 2087.
38. O'Hanley, H.; Buongiorno, J.; McKrell, T.; Hu, L.-W. Measurement and model validation of nanofluid specific heat capacity with differential scanning calorimetry. *Adv. Mech. Eng.* **2012**, *4*, 181079.
39. Zhou, S.-Q.; Ni, R. Measurement of the specific heat capacity of water-based Al_2O_3 nanofluid. *Appl. Phys. Lett.* **2008**, *92*, 1–3.
40. Zhou, L.-P.; Wang, B.-X.; Peng, X.-F.; Du, X.-Z.; Yang, Y.-P. On the specific heat capacity of CuO nanofluid. *Adv. Mech. Eng.* **2010**, *2010*, 1–4.